UC Berkeley
UC Berkeley Previously Published Works

Title

Flow-cytometric analysis of human monocyte subsets targeted by Mycobacterium bovis BCG before granuloma formation

Permalink

Journal

Pathogens and Disease, 76(8)

ISSN

0928-8244

Authors

Delcroix, Melaine
Heydari, Kartoosh
Dodge, Ren
et al.

Publication Date

2018-11-01

DOI

10.1093/femspd/fty080

Peer reviewed

RESEARCH ARTICLE

Flow-cytometric analysis of human monocyte subsets targeted by *Mycobacterium bovis* BCG before granuloma formation

Melaine Delcroix[1], Kartoosh Heydari[2], Ren Dodge[1] and Lee W. Riley[1,*]

[1]Division of Infectious Disease and Vaccinology, 530E Li Ka Shing, School of Public Health, University of California, Berkeley, 94720, USA and [2]LKS Flow Cytometry Core, Cancer Research Laboratory, University of California, Berkeley, CA 94720, USA

*Corresponding author: Division of Infectious Disease and Vaccinology, 530E Li Ka Shing, School of Public Health, University of California, Berkeley, 94720, USA. Tel: +510-642-9200; E-mail: lwriley@berkeley.edu

One sentence summary: This study examines the early interaction of a vaccine strain of *Mycobacterium bovis* (BCG) and immune cells in the formation of granulomas *in vitro*.

Editor: Patrick Brennan

ABSTRACT

Infection with *Mycobacterium tuberculosis* (Mtb) is characterized by an inflammatory response resulting in the formation of granulomas. These tight aggregates of immune cells play an important role in bacterial containment and in the eventual outcome of infection. Monocytes are a major component of the early immune response to Mtb and contribute to the cellular matrix of the newly forming granuloma. Therefore, defining which monocyte subset is the target of mycobacterial infection is critical. Here, we describe a flow-cytometry-based assay to analyze infectivity *in vitro* of monocyte subsets by *Mycobacterium bovis* BCG before granuloma formation. We identified CD14$^+$CD16$^-$ monocytes as the main target of infection in peripheral blood mononuclear cells from six healthy donors. CD14$^+$CD16$^+$ monocytes displayed the lowest infection rates and remained uninfected in some donors. We found that a longer infection time resulted in an increase of the percentage of monocytes infected and of the number of granulomas produced. We did not observe changes in monocyte cell death or subset expansion upon infection. Future experiments with our *in vitro* method could help define Mtb infectivity of monocyte subsets. Our study provides a platform to investigate how early infection of different monocyte subsets may alter granuloma formation and outcomes of Mtb infection.

Keywords: *Mycobacterium*; monocyte subsets; *in vitro* granuloma; flow cytometry

INTRODUCTION

Mycobacterium tuberculosis (Mtb) infection is characterized by the formation of compact and multicellular host structures called granulomas. These aggregates form in response to the phagocytosis of Mtb by alveolar macrophages and other cells which triggers pro-inflammatory signals (Flynn *et al.* 2011). Granulomas are mainly comprised of mature and differentiated macrophages surrounded by lymphocytes. They function both as a niche for the bacteria to establish a robust infection and as a host protective structure that restrains bacterial growth and spread (Ramakrishnan 2012). Proper functioning of granulomas determines whether the infection will stay contained or progress to active disease (Flynn *et al.* 2015). Much of research effort has focused on understanding granuloma formation and maintenance in an attempt to unravel the mechanisms of

disease progression and subsequently develop methods to control tuberculosis (TB).

It has now become evident that the first steps of granuloma formation are critical for the eventual outcome of the infection (Cadena, Flynn and Fortune 2016). Studies in animal models have implicated interactions of mycobacteria with early innate mechanisms in newly emerging caseous granulomas (Turner, Basaraba and Orme 2003; Lin *et al.* 2006). Work in zebrafish infected with *Mycobacterium marinum* has shown how bacteria exploit macrophage death during the early innate immune stages of granuloma formation to proliferate and disseminate throughout the host (Davis and Ramakrishnan 2009). Srivastava *et al.* demonstrated that Mtb infects diverse myeloid cell subsets in the lung during the early phase of infection in a mouse model (Srivastava, Ernst and Desvignes 2014). It was then proposed that, since individual cell subsets exhibit distinct functional properties, early cell recruitment skewed toward one subset or another will likely dictate granuloma response to Mtb. Local differences in forming granulomas would ultimately influence the overall outcome of infection.

Immunological events following Mtb infection include an early recruitment of monocytes from neighboring blood vessels to the site of infection in response to inflammatory signals (Flynn *et al.* 2011; Mattila *et al.* 2013). These monocytes contribute to the cellular matrix of the early granuloma (Russell *et al.* 2009). They are a source of myeloid DCs, alveolar macrophages and recruited interstitial macrophages. Importantly, Srivastava *et al.* showed that a small but constant percentage of monocytes in the mouse lung were infected with Mtb throughout the infection (Srivastava, Ernst and Desvignes 2014).

Monocyte population is highly heterogeneous and comprises three distinct functional subsets delineated by the cell surface expression of CD14 and CD16: the most abundant classical CD14$^+$CD16$^-$ (CD14$^+$), intermediate CD14$^+$CD16$^+$ and non-classical CD14^{dim}CD16$^+$ (CD16$^+$) monocytes (Ziegler-Heitbrock *et al.* 2010). Alterations in monocyte subsets and expansion of CD16$^+$ monocytes have been described in patients with TB and correlated with disease severity (Sanchez *et al.* 2006; Balboa *et al.* 2011). In the context of Mtb infection, CD16$^+$ monocytes have been shown to be dramatically impaired in their capacity to differentiate into functional DCs or macrophages; to produce more TNF-α and less IL-10; to exhibit lower phagocytic capacity; and to be more prone to cell death in response to infection (Castano, Garcia and Rojas 2011; Balboa *et al.* 2013). Lastrucci *et al.* demonstrated that, in the presence of conditioned media from Mtb-infected human macrophages, monocytes differentiated into CD16$^+$CD163$^+$MerTK$^+$pSTAT3$^+$ cells exhibiting high protease-dependent motility, pathogen permissivity and immunomodulatory activity (Lastrucci *et al.* 2015). A study in a transfer mouse model showed that CD16$^-$ monocytes displayed a higher lung migration index, promoted leukocyte recruitment to the lungs and decreased lung bacterial load in comparison with CD16$^+$ monocytes upon infection with Mtb (Balboa *et al.* 2015). Balboa *et al.* proposed that monocyte subsets are committed to precise functions in the infected lung and therefore contribute differentially to the early immune response against Mtb (Balboa *et al.* 2013; Balboa *et al.* 2015).

Although the influx of monocytes into the lungs appears to be a major component of the early immune events following infection with Mtb, the contribution of each monocyte subset in the granulomatous response remains poorly explored. A first step towards understanding how infection of different monocyte subsets would alter granuloma function is to define which monocyte subset is the target of mycobacterial infection. The non-pathogenic *Mycobacterium bovis* BCG strain has proven to be a useful model to study the granulomatous response to mycobacterial infection (Seitzer and Gerdes 2003; Puissegur *et al.* 2004; Rhoades *et al.* 2005). Here, we have exploited the ability of *M. bovis* BCG to infect human monocytes and produce granulomas *in vitro* to develop a new assay to address *Mycobacterium* infectivity of monocyte subsets. We propose a flow-cytometry-based analysis to define monocyte populations infected with *M. bovis* BCG in an *in vitro* infection model of peripheral blood mononuclear cells (PBMCs) leading to granuloma formation. This assay also enabled us to assess infection rates, cell death rates and overall monocyte subset composition upon infection prior to granuloma formation.

MATERIALS AND METHODS

Ethics

Human peripheral blood was obtained from healthy donors at the University of California, Berkeley. The study was approved by the Institutional Review Board of the University of California, Berkeley. All blood donors provided written informed consent. Five of the blood donors had previously been vaccinated with BCG but all were negative by the PPD skin test.

Bacterial strains and growth conditions

Mycobacterium bovis BCG Pasteur was obtained from the ATCC. *Mycobacterium bovis* BCG Pasteur constitutively expressing the green fluorescent protein (GFP) was a gift from the laboratory of Dr. Sarah Stanley. *Mycobacterium bovis* BCG transformed with the reporter plasmid pCHARGE3 (Addgene plasmid # 24 658) and expressing Turbo-635 was kindly provided by Michael Schump (Carroll *et al.* 2010). Bacteria were grown at 37°C in Middlebrook 7H9 medium (Difco) supplemented with 10% ADC (0.5 g/l BSA, 2g/l dextrose and 0.08 g/l NaCl), 0.05% Tween-80 and 0.5% glycerol.

Isolation of PBMCs

Whole blood was collected in Vacutainer tubes with sodium heparin anticoagulant reagent (BD Biosciences) and processed immediately for PBMC isolation. Blood was diluted 1:1 with PBS, layered onto Ficoll-Paque PREMIUM (GE Healthcare) and processed according to manufacturer's instructions. Isolated PBMCs were frozen at 10^7 cells per ml in fetal bovine serum (FBS, Mediatech, VA) with 10% dimethyl sulfoxide. When needed, PBMCs were thawed, washed and resuspended in complete RPMI (cRPMI) containing 10% FBS and 2 mM L-glutamine. Cells rested for 1 hr at 37°C with 5% CO_2 before we proceeded with cell count (trypan blue dye exclusion method) and infection.

Infection

Bacterial cultures with an OD_{600} of 0.5–0.6 were spun down at 50 $\times$ *g* for 5 min to remove clumps. Supernatant was centrifuged at 1900 $\times$ *g* for 5 min. Bacterial pellets were washed once and resuspended in phosphate-buffered saline (PBS). Required strain of *M. bovis* BCG was added to PBMCs at a multiplicity of infection (MOI) of 1:100 in cRPMI. Infected cells and uninfected cells were kept at 37°C in 5% CO_2 incubator. Following 2- and 6-hr incubations, PBMCs were seeded to produce granulomas or immunostained for flow cytometry.

Formation of *in vitro* granulomas

Following infection with *M. bovis* BCG expressing Turbo-635, PBMCs were washed with PBS and seeded onto an extracellular matrix (ECM), pH 7.0, containing 0.75 mg/ml type I bovine collagen (Purecol, Advanced Biomatrix) and 1.25μg/ml bovine fibronectin (Sigma) in cRPMI (Kapoor *et al.* 2013; Parasa *et al.* 2014). Before adding cells, 250 μl ECM were pipetted onto each 12-well Costar Transwell insert (Corning). Plates were incubated for 2 hr at 37°C to solidify ECM and 6×10^5 PBMCs were seeded per insert. cRPMI was added in the outer well and seeded PBMCs were incubated at 37°C in 5% CO_2 incubator. After 24 hr, medium in lower chamber was changed and 300 μl medium added to insert.

Granuloma staining for confocal imaging

PBMCs in Transwells were fixed overnight at 4°C in 4% formaldehyde. Following two PBS washes, membranes of inserts were cut out. Cells were then stained for actin for 2 hr in 2X CytoPainter Phalloidin-iFluor 488 reagent (ABCAM); or for lipid bodies for 1 hr in 1X Bodipy 493/503 (Invitrogen); or incubated with α-CD3 (T-cell marker) polyclonal rabbit and α-CD68 (KP1; macrophage marker) mouse monoclonal anti-human antibodies (Fisher) overnight followed by 1-hr incubation with secondary antibodies goat anti-rabbit IgG, Alexa Fluor 488 and goat anti-mouse IgG1, Alexa Fluor 633, respectively. Secondary-antibody-only controls were run in parallel. After two PBS washes, membranes were mounted onto microscope slides in Prolong Gold antifade reagent with DAPI (Molecular Probes).

Granuloma counting and measurement

Following staining with phalloidin, each membrane was scanned on the widefield DeltaVision Elite microscope (GE Healthcare) under GFP filter. Images were then analyzed on Bitplane Imaris (Oxford Instruments) with the Surfaces function. To count and measure aggregates with an area of at least 6000 μm^2, the following parameters were used: source channel at 523 nm; Smooth option selected with Surface Detail at 10 μm; Background Subtraction with Sphere Diameter at 100 μm; threshold was adjusted manually to cover individual granulomas; surfaces were filtered to include areas larger than 1200 voxels. The Surfaces function rendered 3-D objects with two sides and thickness of 1 voxel, so the 2-D cross-sectional area is the total surface area divided by two.

Confocal imaging

Cells were imaged on a Zeiss LSM710 confocal microscope. DAPI fluorescence was excited with a 405–430 nm diode laser line and collected with a 410–490 nm emission filter. For Phalloidin-iFluor 488 and Alexa Fluor 488, we used the 488 nm line of an Argon laser and fluorescence emission was collected between 500 and 550 nm. For Turbo-635, we used the 594 nm line of a Helium–Neon laser and emission between 600 and 650 nm was collected. For Alexa Fluor 633, we used the 633 nm line of a Helium–Neon laser and emission above 650 nm was collected. Images were acquired on a Zeiss LSM710 confocal microscope and processed on ImageJ (Schindelin *et al.* 2012).

Immunolabeling for flow cytometry

Following infection with *M. bovis* BCG expressing GFP, cells were washed in PBS and labeled with Live/Dead fixable Blue (Life Technologies) according to manufacturer's instructions. Cells were then incubated in a PBS blocking buffer containing 5% FBS for one hour at 4°C. Cells were stained in blocking buffer in the dark for 30 min at 4°C with a cocktail of the following titrated antibodies: Pacific Blue α-CD14 (HCD14), PE/Cy7 α-CD16 (3G8), APC/Cy7 α-HLA-DR (L243), APC α-CD56 (MEM-188, Life Technologies), PerCP/Cy5.5 α-CD3 (OKT3) and PerCP/Cy5.5 α-CD19 (HIB19). Cells were washed once in PBS, fixed overnight at 4°C in 4% formaldehyde and resuspended in PBS prior to flow cytometry. All antibodies were from Biolegend unless specified.

Flow cytometry

Data were collected with FACSDiva software on a Fortessa flow cytometer (BD Biosciences) with five laser lines (355, 405, 488, 561 and 640 nm). At least 10^6 events were collected for each sample. Compensation matrix was calculated automatically with FACSDiva software. Compensation controls included: unstained PBMCs, single-stained PBMCs, a 1:1 mixture of Live/Dead fixable blue-stained live PBMCs and formaldehyde-fixed PBMCs, and FITC-labeled Calibrite beads (BD) for cells infected with GFP-expressing bacteria. Data were analyzed on Flow Jo software (TreeStar). A first ample gate based on size and granularity included monocytes and lymphocytes. Side-scatter and forward-scatter width and height ratios were employed to exclude cell doublets from analysis. Fluorochrome minus one (FMO) controls, where one antibody or probe was left out of the cocktail in turn, helped adjust gates to delineate positive and negative populations.

Statistical analysis

Scatter plots were generated with the ggplot2 package in R (Team 2013). We performed Wilcoxon ranked-sign tests with the R function Wilcox test to compare the composition of monocyte population in 2- vs 6-hr infections and in uninfected vs infected PBMCs.

RESULTS

Formation of *in vitro* granulomas

As we wanted to analyze the infectivity of monocytes in the context of granuloma formation, we first had to establish which conditions of infection led to the formation of granulomas *in vitro*. We infected PBMCs with *M. bovis* BCG expressing the reporter Turbo-635 at MOI of 1:1000, 1:100 or 1:10 for 2 or 6 hr. To assess the overall infection profile for each condition and donor, we scanned the whole membranes bearing the infected cells in collagen matrix for actin staining and counted and measured granulomas. Parameters on Imaris were set to remove the numerous aggregates composed of few cells and we then quantified the size and numbers of aggregates above 6000 μm^2. We found that an MOI of 1:100 produced the largest and most stable granuloma-like structures. Fig. 1A shows the number and size of the aggregates at day 11, when aggregates are the largest and most numerous before the structures start breaking down. Mean area was between 6000 and 10 000 μm^2 for all donors except for donor 3010 after 2-hr infection when large structures above 20 000 μm^2 were formed. We observed variation between donors in the number of granulomas produced, ranging from 1 to 19 for 2-hr incubations while 6-hr incubations yielded 15 to 35 aggregates. Six-hr infection of PBMCs from donors 101 and 3010 yielded the most granulomas with 35 aggregates of at least

(A) Number and size of granulomas produced *in vitro*
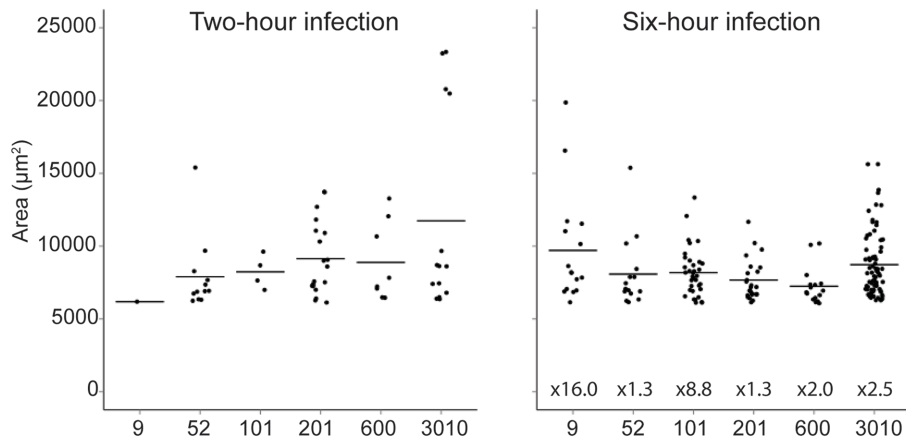
(B) Progression of granuloma structures
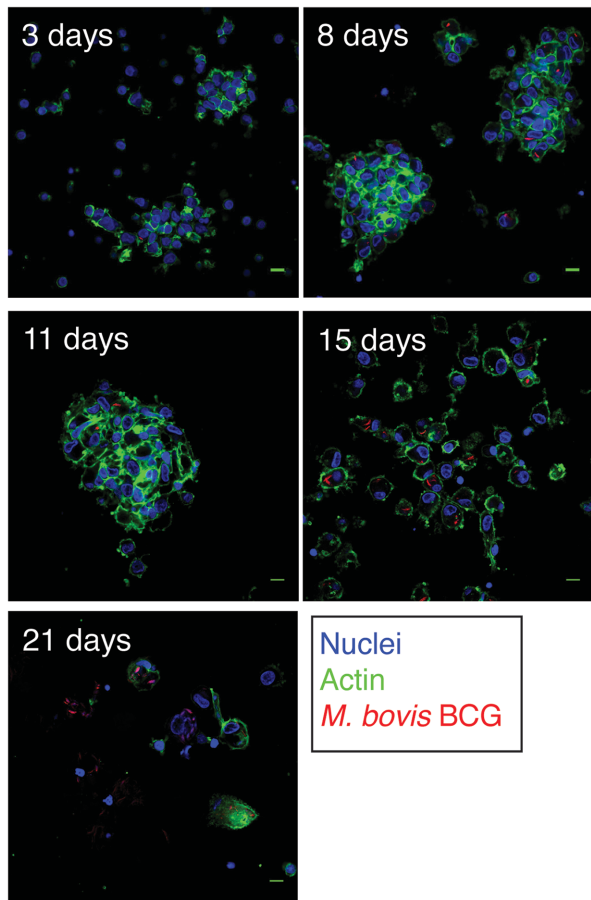
(C) Hallmarks of granuloma structures
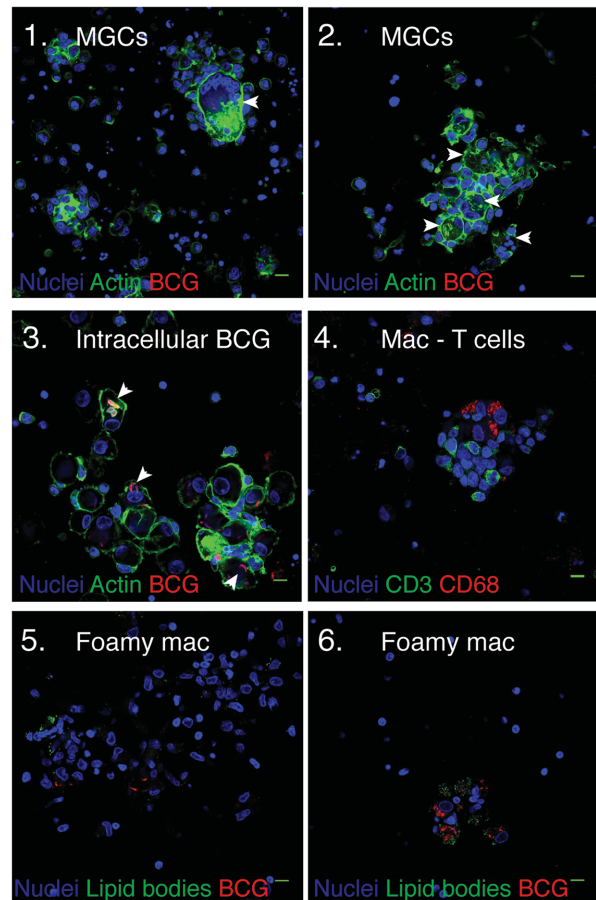
Figure 1. Infection of PBMCs with Turbo-635-expressing *M. bovis* BCG resulted in the formation of granuloma-like structures. **(A)**, Number and size of aggregates formed at day 11 post-infection. Following 2- and 6-hr infection at an MOI of 1:100, PBMCs from donors 9, 52, 101, 201, 600 and 3010 were seeded onto a collagen matrix and incubated for 11 days. Actin staining with phalloidin revealed the whole granuloma structures that were imaged, counted and measured. Mean area of aggregates is shown for each donor. Fold increase in number of aggregates over incubation time is included in second plot. **(B)**, Nascent aggregates seen at day 3 develop into larger, compact and multilayered structures at days 8 and 11. At day 15, aggregates become looser and composed of more highly infected cells resulting in granuloma breakdown and extracellular bacteria (day 21). Nuclei were stained with DAPI (blue) and actin with phalloidin-iFluor 488 (green); *M. bovis* BCG expresses Turbo-635 (red). **(C)**, Granuloma hallmarks include multinucleated giant cells (1,2, white arrows—MGCs), intracellular bacteria (red), intracellular bacteria (3, white arrows), recruitment of CD68^{+} macrophages (4, red) and CD3^{+} lymphocytes (4, green) and foamy macrophages with Bodipy 493/503-stained lipid bodies (green) in large and small aggregates (5,6). Scale bars: 10 μm.

6000 μm^2. When looking at the effect of a longer incubation time of PBMCs with *M. bovis* BCG, we did not see larger aggregates formed after 6-hr infection but for all donors, we did find an increase in the number of granulomas of 1.3- to 16.0-fold. Donors 9 and 101 exhibited the highest increase in aggregates produced. No cellular aggregation was observed in uninfected cell cultures throughout the course of the study. PBMC infection at an MOI of 1:1000 resulted in the aggregation of few cells while infection at an MOI of 1:10 resulted in cell death (as assessed by the weakness of phalloidin-iFluor 488 signal), no cell aggregation and extracellular clumps of *M. bovis* BCG (data not shown).

The structure of the aggregates formed was then analyzed by confocal microscopy. Fig. 1B illustrates the typical progression of granuloma formation following 6-hr incubation of PBMCs with *M. bovis* BCG at an MOI of 1:100 over 3 weeks post-infection. Imaging of granulomas at day 3 revealed nascent aggregates with few intracellular bacteria. At days 8 and 11, larger, compact and multilayered structures with a restricted number of intracellular bacteria were observed. At day 15, aggregates progressed into looser aggregates composed of more highly infected cells. At a later stage, at day 21 post-infection, most granulomas had fallen apart and clumps of extracellular bacteria could be seen throughout the collagen matrix. Panel 1C illustrates the granuloma hallmarks we observed in our model. Multinucleated giant cells (MGCs) were found within aggregates composed of few cells at eight or more days post infection in each infection. Some MGCs contained a large number of nuclei tightly organized in a ring close to the membrane, with intracellular bacteria visible as shown in image 1. We also observed smaller/nascent MGCs with two to three nuclei as depicted in image 2. Immunostaining for CD68, a macrophage-specific marker, was performed and confirmed that the MGC belonged to the monocyte/macrophage lineage (data not shown). Vacuolar distribution of bacteria residing within phalloidin-stained vesicles was visible in some cells (image 3). Immunostaining of aggregates showed the recruitment of cells positive for CD68, macrophages and cells with little cytoplasm positive for CD3, a T cell marker (image 4). Finally, we confirmed the presence of foamy macrophages in larger structures with cells positively stained for lipid bodies (image 5). We also found heavily infected cells with a high number of lipid bodies as shown in image 6.

We decided to pursue our *in vitro* infection assays with an MOI of 1:100 for 6 hr as they produced at least 15 stable aggregates with an area above 6000 μm^2 and with the major characteristics of granulomas associated with *Mycobacterium* infection. As increasing the time of infection led to more granulomas produced, we also conducted 2-hr infections to investigate changes in monocyte infection over time.

M. bovis BCG infectivity of monocyte subsets

To determine which monocyte subset(s) become(s) infected with *M. bovis* BCG, we isolated PBMCs from six healthy blood donors and infected them with *M. bovis* BCG expressing the reporter protein GFP for 2 and 6 hr. Human monocyte subsets can be distinguished by flow cytometry based on the expression of the cell surface markers CD14 and CD16 (Ziegler-Heitbrock *et al.* 2010). Fig. 2 illustrates the gating strategy used to discriminate infected monocytes and to identify the subsets they belong to. Following exclusion of doublets, dead cells, T cells, B cells, CD16$^+$CD56$^+$ NK cells and HLA-DR$^-$ cells, the resultant population was visualized on a plot based on the expression of CD14 and CD16 to delineate monocyte population. Within monocytes, cells infected with *M.*

bovis BCG expressing GFP were identified based on the FMO control PBMCs infected with wild-type *M. bovis* BCG (Fig. 2H).

Fig. 3 represents the subset composition of infected monocytes. We found that infection rates among monocytes reached 0.5% to 0.8% after 2 hr and 2.6% to 5.0% after 6 hr, with a 3.3 to 7.0 fold increase in the percentage of monocyte infected over time. Monocyte immunophenotyping based on the expression of CD14 and CD16 on GFP$^+$ monocytes for each donor showed that CD14$^+$ monocytes were the main target, representing 96.6% to 100.0% of infected monocytes after 2 hr of infection. CD14$^+$ cells constituted 98.0% to 99.7% of infected monocytes after 6 hr of infection. Two additional biological replicates were run in independent experiments on PBMCs from donor 9 infected for 2 hr. These infections yielded consistent monocyte infection rates of 0.8% and 1.2% with 98.8% and 98.6% of infected monocytes belonging to the CD14$^+$ subset, respectively (data not shown). Infected CD16$^+$ monocytes were present in PBMCs from all donors after 6 hr of infection and accounted for 0.3% to 1.6% of all infected monocytes. None of the donors had any CD14$^+$CD16$^+$ monocytes infected after 2 hr. Following the 6-hr infection, CD14$^+$CD16$^+$ monocytes constituted 0% to 0.9% of infected monocytes.

We calculated the percentage of infected cells within each monocyte subset (Table 1). The proportion of infected cells within each subset increased over the course of infection for all donors, except for CD14$^+$CD16$^+$ monocytes in donors 52 and 201 as they remained uninfected. When comparing infection rates between subsets, we found that CD14$^+$ monocytes exhibited the highest rates for all donors: for instance, for donor 600, CD14$^+$ monocytes were 14 times more infected than CD16$^+$ within 2 hr. Interestingly, we also observed that, while CD16$^+$ cells composed at least 30% of the monocyte population, this cell subset represented only 2.9% and 3.5% of infected monocytes in donors #201 and #600, respectively, after 2 hr of infection (Fig. 3).

Monocyte death following infection with *M. bovis* BCG

As CD16$^+$ cells have been reported to be more prone to cell death than CD14$^+$ monocytes upon infection, we looked at cell death in monocyte populations for each donor following 2- and 6-hr incubations in the presence and absence of *M. bovis* BCG (Table 1) (Castano, Garcia and Rojas 2011). First, we found high variability among donors when comparing monocyte death in infected and uninfected PBMCs: some subjects exhibited decreases in monocyte death while others showed sharp increases upon infection. Similar results were found for overall cell death rates in PBMCs (data not shown). The percentage of CD14$^+$ cells within dead monocytes remained constant in uninfected and infected PBMCs. This subset composed at least 90.0% of the population of dead monocytes. Interestingly, for all donors, infected cells represented a small fraction of the dead monocytes with 0.4% to 4.4% cells found to be GFP$^+$ within this population. Monocyte subset distribution of dead-infected monocytes was similar to that of live-infected monocytes with CD14$^+$ cells representing 100% of dead monocytes after 2 hr of infection and 97.1% to 99.7% after 6 hr.

Composition of monocyte population upon infection with *M. bovis* BCG and over incubation time

As CD14$^+$CD16$^+$ monocytes have been shown to expand upon *in vitro* viral infections (Kwissa *et al.* 2014; Michlmayr *et al.* 2017), we compared the composition of the monocyte population in uninfected PBMCs (data not shown) vs infected PBMCs for each
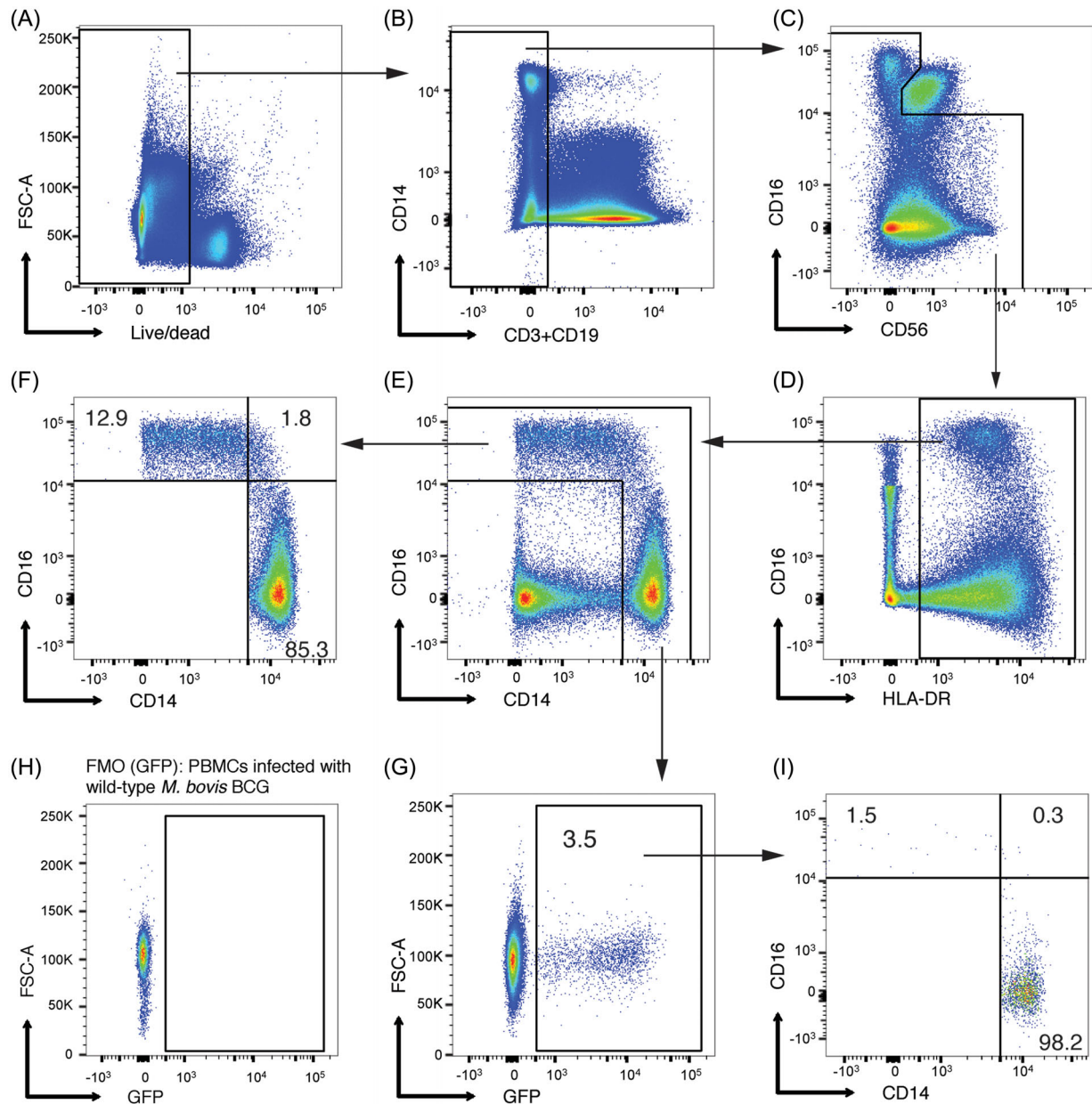
Figure 2. Representative dot plots of the gating strategy used to identify CD14+, CD14+CD16+ and CD16+ monocytes infected with *M. bovis* BCG expressing GFP. Cells were pre-gated based on size and granularity to include PBMCs. Following doublet exclusion, monocyte and lymphocyte populations are first gated for viability. **(A)**, Within live cells, stepwise gating of daughters populations was performed to exclude T cells and B cells based on CD3 and CD19 expression, respectively **(B)**, CD56+CD16+ NK cells **(C)**, and HLA-DR− cells **(D)**, Cells are then viewed on a CD14 vs CD16 plot and a gate is drawn around the monocyte population **(E)**, divided into CD14+, CD14+CD16+ and CD16+ subsets **(F)**, Gate for monocytes infected with *M. bovis* BCG expressing GFP **(G)**, is based on the FMO control PBMCs infected with wild-type *M. bovis* BCG **(H)**, Infected monocytes are then broken down into their subsets to determine which subset(s) is/are infected **(I)**.

donor (Fig. 3). We grouped samples in two sets, each including 2- and 6-hr incubations: 12 uninfected PBMC samples vs 12 infected PBMC samples. We ran a Wilcoxon signed-rank test to compare the two sets and found that infection did not significantly affect the proportion of monocyte subsets: CD16+, V = 55, P-value = 0.2094; CD14+, V = 21, P-value = 0.2858; CD14+CD16+, V = 21.5, P-value = 0.1696. We also looked at changes over time by comparing monocyte populations at 2-hr and 6-hr incubations. All donors saw a decrease in the percentage of CD16+ monocytes and an increase in the percentage of CD14+ monocytes between 2 and 6 hr incubations (except for uninfected PBMCs for donor #9). We found that during incubation time the

CD14+CD16+ population expanded in all donors. A Wilcoxon signed-rank test indicated that the composition of monocyte population was significantly different at 2 and 6 hr with the following values: CD16+, V = 76, P-value = 0.004; CD14+, V = 8, P-value = 0.015; CD14+CD16+, V = 0, P-value = 0.002.

DISCUSSION

Given the critical role of monocytes in the early granuloma response to Mtb infection, it is important to understand how monocyte subsets can differentially support the formation of granuloma structures. Here, we described a flow-cytometry-
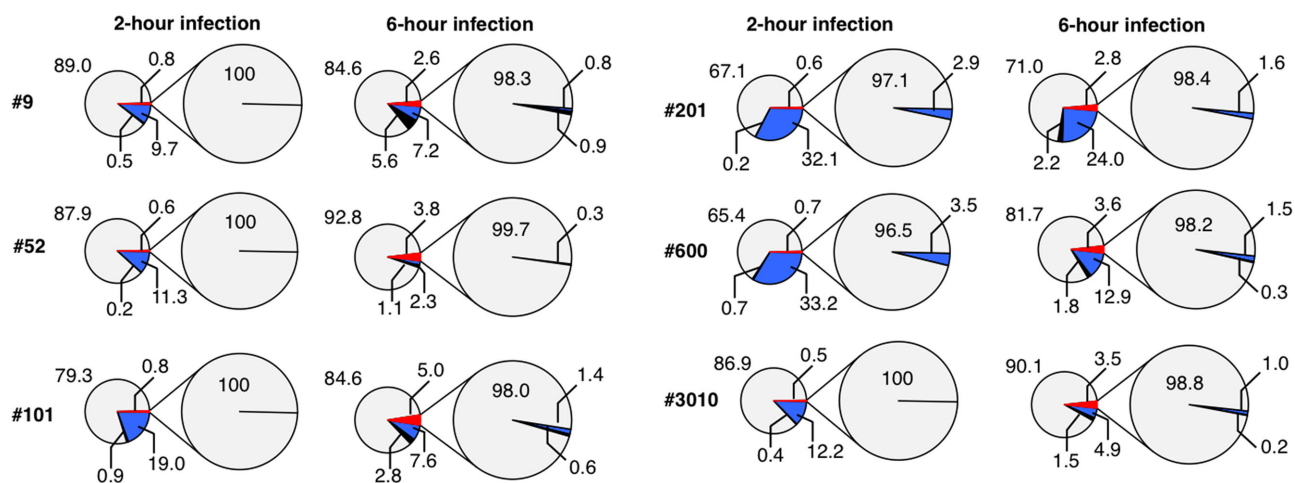
Figure 3. Composition of infected monocyte population after 2- and 6-hr infections of PBMCs with GFP-expressing *M. bovis* BCG. Smaller pie charts depict the proportion of the CD14$^+$ (grey), CD14$^+$CD16$^+$ (black) and CD16$^+$ (blue) cells within the monocyte population for each donor. The red pie slice represents the population of infected monocytes broken down into CD14$^+$, CD14$^+$CD16$^+$ and CD16$^+$ subsets in the larger pie.

Table 1. Infection and death cell rates of monocytes following 2- and 6-hr infections of PBMCs with GFP-expressing *M. bovis* BCG. Live cells were pre-gated on monocyte subsets and the percentage of infected cells (GFP$^+$) in each subset was calculated for each donor. To investigate cell death in monocytes, cells were pre-gated on dead PBMCs, followed by gating out lineage-positive cells, NK cells and HLA-DR-negative cells. For each donor, percentages of CD14$^+$ cells and GFP$^+$ cells within the dead monocyte population are shown. Within GFP$^+$ dead monocytes, the proportion of CD14$^+$ subset is shown.

	2-hr infection/incubation						6-hr infection/incubation					
	#9	#52	#101	#201	#600	#3010	#9	#52	#101	#201	#600	#3010
GFP$^+$ cells within												
CD16$^+$ monocytes	0.0	0.0	0.0	0.1	0.1	0.0	0.3	0.5	0.9	0.2	0.4	0.7
CD14$^+$CD16$^+$ monocytes	0.0	0.0	0.0	0.0	0.0	0.0	0.4	0.0	1.0	0.0	0.6	0.4
CD14$^+$ monocytes	0.9	0.7	0.9	0.9	1.0	0.6	2.9	3.9	5.5	3.7	4.1	3.7
Monocytes within dead PBMCs												
−*M. bovis* BCG	49.9	47.8	32.3	13.5	16.4	40.7	8.3	17.4	17.1	9.14	15.3	29.4
+*M. bovis* BCG	32.2	36.5	42.5	19.9	38.8	29.5	16.4	28.7	27.6	12.1	3.11	20.8
CD14$^+$ within dead monocytes												
−*M. bovis* BCG	98.7	99.1	98	96.3	90.0	98.8	95.2	99.2	97.4	98	93.9	98.7
+*M. bovis* BCG	98.8	99.2	97.3	97.4	94	98.8	96.9	99.4	96.9	93.1	95	98.6
GFP$^+$ cells within dead monocytes	0.6	0.4	0.8	0.8	0.3	0.4	1.9	2.6	4.4	2.9	3.9	2.8
CD14$^+$ cells within GFP$^+$ dead monocytes	100	100	100	100	100	100	99.0	99.7	99.2	98.6	97.1	99.5

based assay to define which monocyte subset(s) is/are the main target(s) of *Mycobacterium* infection before granuloma formation. We first defined the conditions of infection that produced stable aggregates exhibiting the hallmarks of tuberculous granulomas. We then applied these infection settings to our flow cytometry assay. Our results showed that we could clearly identify infected monocyte subsets following *in vitro* infection of PBMCs with GFP-expressing *M. bovis* BCG. As our study included a restricted number of blood donors (six), we did not run any statistical analysis on the percentages of infected monocyte subsets. However, we found that CD14$^+$ monocytes were overwhelmingly the main target of *M. bovis* BCG, representing at least 96.6% of infected monocytes in all six donors. Monocyte subset infection rates for each donor suggest that the infection was preferentially biased towards CD14$^+$ monocytes. Indeed, even in donors with CD16$^+$ cells representing more than 30% of their monocyte populations, this subset only constituted up to 3.5% of infected monocytes. We also found that CD14$^+$CD16$^+$ monocytes remained uninfected in some donors even after 6 hr of infection. Interestingly,

CD14$^+$ monocytes have been reported to play an active role in Mtb infection. It highly expresses the chemokine receptor CCR2 (Wong *et al.* 2011). Work in mouse chimera models to study first stages of infection showed that bacteria were likely transported from the lungs or granulomas to lung-draining lymph nodes by monocytes expressing CCR2 (Samstein *et al.* 2013; Orme, Robinson and Cooper 2015). A study in a transfer mouse model has also implicated CD14$^+$ monocytes in early leukocyte recruitment to the lungs and in decreased lung bacterial load upon infection with Mtb (Balboa *et al.* 2015). As increased cell death in sorted CD16$^+$ monocytes upon infection had been described, we compared subset distribution in dead- and live-infected monocytes for each donor and found that they were similar (Castano, Garcia and Rojas 2011). Dead-infected CD16$^+$ monocytes did not compensate for CD14$^+$ infection bias we saw in each of our donors.

To our knowledge, there has only been one published study on *Mycobacterium* infectivity and it was performed with individual infections of CD16$^-$ vs CD16$^+$ sorted and

differentiated monocytes: Castaño *et al.* reported that CD16⁺ monocytes showed a slight decrease in capacity to phagocytose Mtb as they found lower percentages of sorted CD16⁺ monocytes positive for fluorescein diacetate-labeled Mtb following monocyte differentiation for 24 hr and infection at a MOI of 5:1 (Castano, Garcia and Rojas 2011). When comparing our findings to Castaño *et al.*'s, we should emphasize that differences in experimental procedures prevent us from drawing any conclusions on pathogenic *vs* non-pathogenic *Mycobacteria* infectivity. Our approach to explore *Mycobacterium* infectivity of monocyte subsets has several advantages: (i) we subdivided CD16⁺ monocytes into intermediate and non-classical subsets; analyzing CD16⁺ monocytes as a single population would overlook the impact CD14⁺CD16⁺ may have on granuloma formation. This subset has unique features and has been suggested to play a critical role in infection (Ellery *et al.* 2007; Wong *et al.* 2011; Kwissa *et al.* 2014, Michlmayr *et al.* 2017); (ii) we did not perform independent infections for each subset but looked at *Mycobacterium* infectivity in a context where all monocyte subpopulations 'compete' for infection. Infecting sorted monocytes *vs* all PBMCs or infecting independently each monocyte subset represents a different assessment of infectivity; (iii) we were able to look at very early events in infection; (iv) we ran infection assays under conditions yielding stable granulomas *in vitro*. Other groups have looked at later time points in infection, assessing the permissivity to Mtb replication of monocyte subsets purified with immunomagnetic beads (Dhiman *et al.* 2011; Balboa *et al.* 2015). Balboa *et al.* identified CD16⁺ monocytes as more permissive while Dhiman *et al.* reported that Mtb grew more rapidly in CD14⁺ monocytes. Regarding other pathogens, *Leishmania braziliensis* was found to infect a similar percentage of cells in each monocyte subset (Novais *et al.* 2014). Michlmayr *et al.* concluded that CD14⁺CD16⁺ monocytes were the main target of ZIKA virus in an *in vitro* infection of PBMCs from four healthy blood donors, with about 60% of infected monocytes belonging to this subset. They also found that CD14⁺CD16⁺ monocytes expanding upon infection (Michlmayr *et al.* 2017). In our study, *M. bovis* BCG preferentially infected CD14⁺ monocytes and CD14⁺CD16⁺ monocytes represented less than 1% of infected monocytes. Infectivity of monocyte subsets appears to vary between infectious agents. Our results also showed that monocyte subset distribution remained unchanged upon infection in each donor but revealed that CD14⁺CD16⁺ population expanded over time, regardless of infection. This finding highlights the importance of controlling for incubation times when studying changes in monocyte subsets.

Our study was conducted with *M. bovis* BCG, a vaccine strain has served as a model organism to study granuloma formation but may not reflect what happens with the pathogenic strain Mtb. It also relied on the infection of PBMCs, which differs from infectious events that occur in lungs, where infection of alveolar macrophages leads to the recruitment of monocytes, neutrophils and lymphocytes, resulting in the formation of a granuloma. The distribution of monocyte subsets in the lungs will also differ from that in the peripheral blood and will depend on the level of pulmonary inflammation and on the migration capacity of each monocyte subset. Regardless, when seeding PBMCs infected with *M. bovis* BCG, stable granulomas formed and we observed characteristics of granuloma structures, including intracellular bacteria, macrophage differentiation into MGCs, recruitment of lymphocytes and lipid bodies in macrophages. Thus, the study shows that granuloma formation can be initiated with the infection of a subset of monocyte population. We also found that extending the time of infection increased the percentage of monocytes infected along with the number of granulomas produced. This suggests a role for early recruited monocytes in the formation of granulomas and therefore in the outcome of mycobacterial infection. Infection of monocytes may also be relevant in the context of disseminated mycobacterial infection.

As studying early events in mycobacterial infection in humans is challenging, many research groups rely on the use of *in vitro* model systems to investigate the human context of *Mycobacterial* infection (Fitzgerald *et al.* 2014; Parasa *et al.* 2014). Future use of our flow-cytometry-based assay will help determine which monocyte subsets are the targets of Mtb, probe pathogenic *vs* non-pathogenic mycobacteria infectivity, and compare mutant strains infectivity in *in vitro* granuloma models. Our assay can also be applied to studies where alterations in granuloma formation were observed. For instance, Guirado *et al.* found that, following Mtb infection, granuloma formation was altered in PBMCs from latently infected individuals, which exhibited accelerated cell recruitment and better control of bacillary load over time compared to PBMCs from naïve donors (Guirado *et al.* 2015). Such studies could benefit from our assay to explore whether changes in infection of monocyte subsets supports the formation of altered granuloma structures.

REFERENCES

Balboa L, Barrios-Payan J, Gonzalez-Dominguez E *et al.* Diverging biological roles among human monocyte subsets in the context of tuberculosis infection. *Clin Sci* 2015;**129**:319–30.

Balboa L, Romero MM, Basile JI *et al.* Paradoxical role of CD16+CCR2+CCR5+ monocytes in tuberculosis: efficient APC in pleural effusion but also mark disease severity in blood. *J Leukoc Biol* 2011;**90**:69–75.

Balboa L, Romero MM, Laborde E *et al.* Impaired dendritic cell differentiation of CD16-positive monocytes in tuberculosis: role of p38 MAPK. *Eur J Immunol* 2013;**43**:335–47.

Cadena AM, Flynn JL, Fortune SM. The importance of first impressions: Early events in *Mycobacterium tuberculosis* infection influence outcome. *MBio* 2016;**7**:e00342–16.

Carroll P, Schreuder LJ, Muwanguzi-Karugaba J *et al.* Sensitive detection of gene expression in mycobacteria under replicating and non-replicating conditions using optimized far-red reporters. *PLoS One* 2010;**5**:e9823.

Castano D, Garcia LF, Rojas M. Increased frequency and cell death of CD16+ monocytes with *Mycobacterium tuberculosis* infection. *Tuberculosis* 2011;**91**:348–60.

Davis JM, Ramakrishnan L. The role of the granuloma in expansion and dissemination of early tuberculous infection. *Cell* 2009;**136**:37–49.

Dhiman R, Bandaru A, Barnes PF *et al.* c-Maf-dependent growth of *Mycobacterium tuberculosis* in a CD14(hi) subpopulation of monocyte-derived macrophages. *J Immunol* 2011;**186**:1638–45.

Ellery PJ, Tippett E, Chiu YL *et al.* The CD16+ monocyte subset is more permissive to infection and preferentially harbors HIV-1 in vivo. *J Immunol* 2007;**178**:6581–9.

Fitzgerald LE, Abendano N, Juste RA *et al.* Three-dimensional in vitro models of granuloma to study bacteria-host interactions, drug-susceptibility, and resuscitation of dormant mycobacteria. *BioMed Res Int* 2014;**2014**:1–8.

Flynn JL, Chan J, Lin PL. Macrophages and control of granulomatous inflammation in tuberculosis. *Mucosal Immunol* 2011;**4**:271–8.

Flynn JL, Gideon HP, Mattila JT *et al.* Immunology studies in non-human primate models of tuberculosis. *Immunol Rev* 2015;**264**:60–73.

Guirado E, Mbawuike U, Keiser TL *et al.* Characterization of host and microbial determinants in individuals with latent tuberculosis infection using a human granuloma model. *mBio* 2015;**6**:e02537–14.

Kapoor N, Pawar S, Sirakova TD *et al.* Human granuloma in vitro model, for TB dormancy and resuscitation. *PLoS One* 2013;**8**:e53657.

Kwissa M, Nakaya HI, Onlamoon N *et al.* Dengue virus infection induces expansion of a CD14(+)CD16(+) monocyte population that stimulates plasmablast differentiation. *Cell Host Microbe* 2014;**16**:115–27.

Lastrucci C, Benard A, Balboa L *et al.* Tuberculosis is associated with expansion of a motile, permissive and immunomodulatory CD16+ monocyte population via the IL-10/STAT3 axis. *Cell Res* 2015;**25**:1333–51.

Lin PL, Pawar S, Myers A *et al.* Early events in *Mycobacterium tuberculosis* infection in cynomolgus macaques. *Infect Immun* 2006;**74**:3790–803.

Mattila JT, Ojo OO, Kepka-Lenhart D *et al.* Microenvironments in tuberculous granulomas are delineated by distinct populations of macrophage subsets and expression of nitric oxide synthase and arginase isoforms. *J Immunol* 2013;**191**:773–84.

Michlmayr D, Andrade P, Gonzalez K *et al.* CD14+CD16+ monocytes are the main target of Zika virus infection in peripheral blood mononuclear cells in a paediatric study in Nicaragua. *Nat Microbiol* 2017;**2**:1462–70.

Novais FO, Nguyen BT, Beiting DP *et al.* Human classical monocytes control the intracellular stage of Leishmania braziliensis by reactive oxygen species. *J Infect Dis* 2014;**209**:1288–96.

Orme IM, Robinson RT, Cooper AM. The balance between protective and pathogenic immune responses in the TB-infected lung. *Nat Immunol* 2015;**16**:57–63.

Parasa VR, Rahman MJ, Ngyuen Hoang AT *et al.* Modeling Mycobacterium tuberculosis early granuloma formation in experimental human lung tissue. *Dis Model Mech* 2014;**7**:281–8.

Puissegur MP, Botanch C, Duteyrat JL *et al.* An in vitro dual model of mycobacterial granulomas to investigate the molecular interactions between mycobacteria and human host cells. *Cell Microbiol* 2004;**6**:423–33.

Ramakrishnan L. Revisiting the role of the granuloma in tuberculosis. *Nat Rev Immunol* 2012;**12**:352–66.

Rhoades ER, Geisel RE, Butcher BA *et al.* Cell wall lipids from *Mycobacterium bovis* BCG are inflammatory when inoculated within a gel matrix: Characterization of a new model of the granulomatous response to mycobacterial components. *Tuberculosis* 2005;**85**:159–76.

Russell DG, Cardona PJ, Kim MJ *et al.* Foamy macrophages and the progression of the human tuberculosis granuloma. *Nat Immunol* 2009;**10**:943–8.

Samstein M, Schreiber HA, Leiner IM *et al.* Essential yet limited role for CCR2+ inflammatory monocytes during Mycobacterium tuberculosis-specific T cell priming. *Elife* 2013;**2**:e01086.

Sanchez MD, Garcia Y, Montes C *et al.* Functional and phenotypic changes in monocytes from patients with tuberculosis are reversed with treatment. *Microbes Infect* 2006;**8**:2492–500.

Schindelin J, Arganda-Carreras I, Frise E *et al.* Fiji: an open-source platform for biological-image analysis. *Nat Methods* 2012;**9**:676–82.

Seitzer U, Gerdes J. Generation and characterization of multicellular heterospheroids formed by human peripheral blood mononuclear cells. *Cells Tissues Organs* 2003;**174**:110–6.

Srivastava S, Ernst JD, Desvignes L. Beyond macrophages: the diversity of mononuclear cells in tuberculosis. *Immunol Rev* 2014;**262**:179–92.

Team RC. *R: A language and environment for statistical computing*. Vienna: R Foundation for Statistical Computing, 2013.

Turner OC, Basaraba RJ, Orme IM. Immunopathogenesis of pulmonary granulomas in the guinea pig after infection with Mycobacterium tuberculosis. *Infect Immun* 2003;**71**:864–71.

Wong KL, Tai JJ, Wong WC *et al.* Gene expression profiling reveals the defining features of the classical, intermediate, and non-classical human monocyte subsets. *Blood* 2011;**118**:e16–31.

Ziegler-Heitbrock L, Ancuta P, Crowe S *et al.* Nomenclature of monocytes and dendritic cells in blood. *Blood* 2010;**116**:e74–80.